Supplementary Information for:

A Constant Current Triboelectric Nanogenerator Achieved by Hysteretic and Ordered Charge Migration in Dielectric Polymers

Huiyuan Wu, Jian Wang, Shaoke Fu, Chuncai Shan, Qionghua Zhao, Kaixian Li, Gui Li, Qianjin Mu, Xue Wang*, and Chenguo Hu*
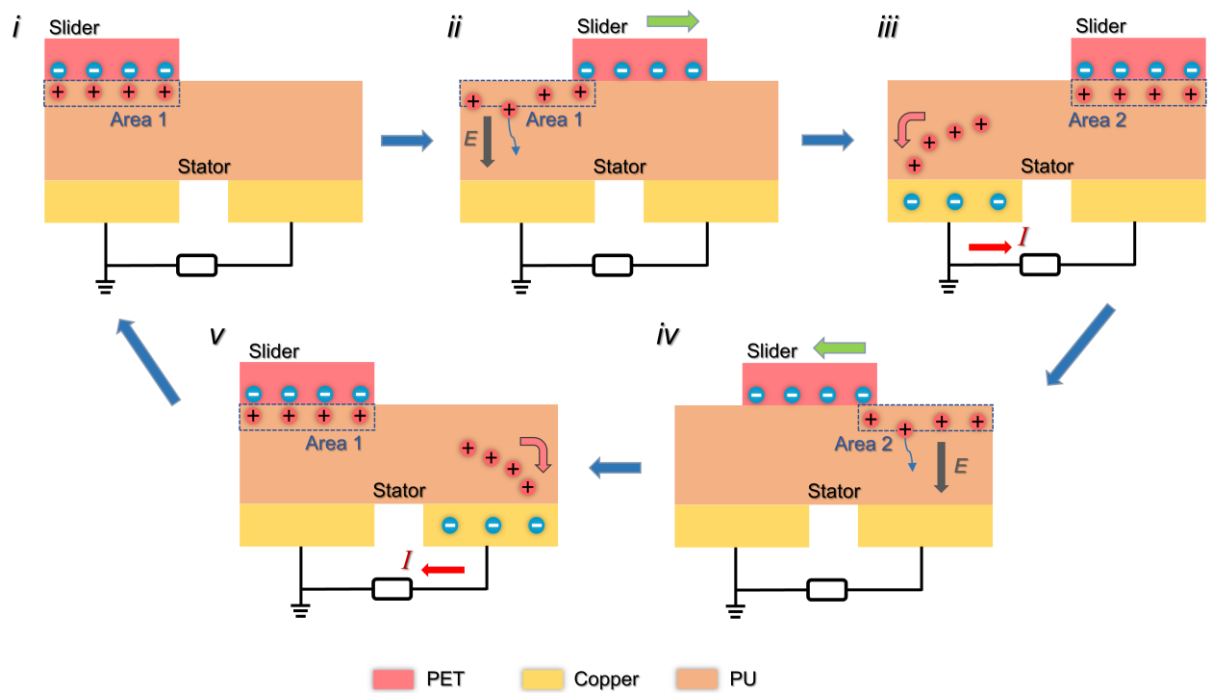
Contents:

Figure S1. Detailed working principle diagram of HSC-TENG.

Figure S2. Detailed explanations and comparisons of different types of SC-TENGs.

Initial   **24 hour**   **48 hour**

72 hour   **96 hour**
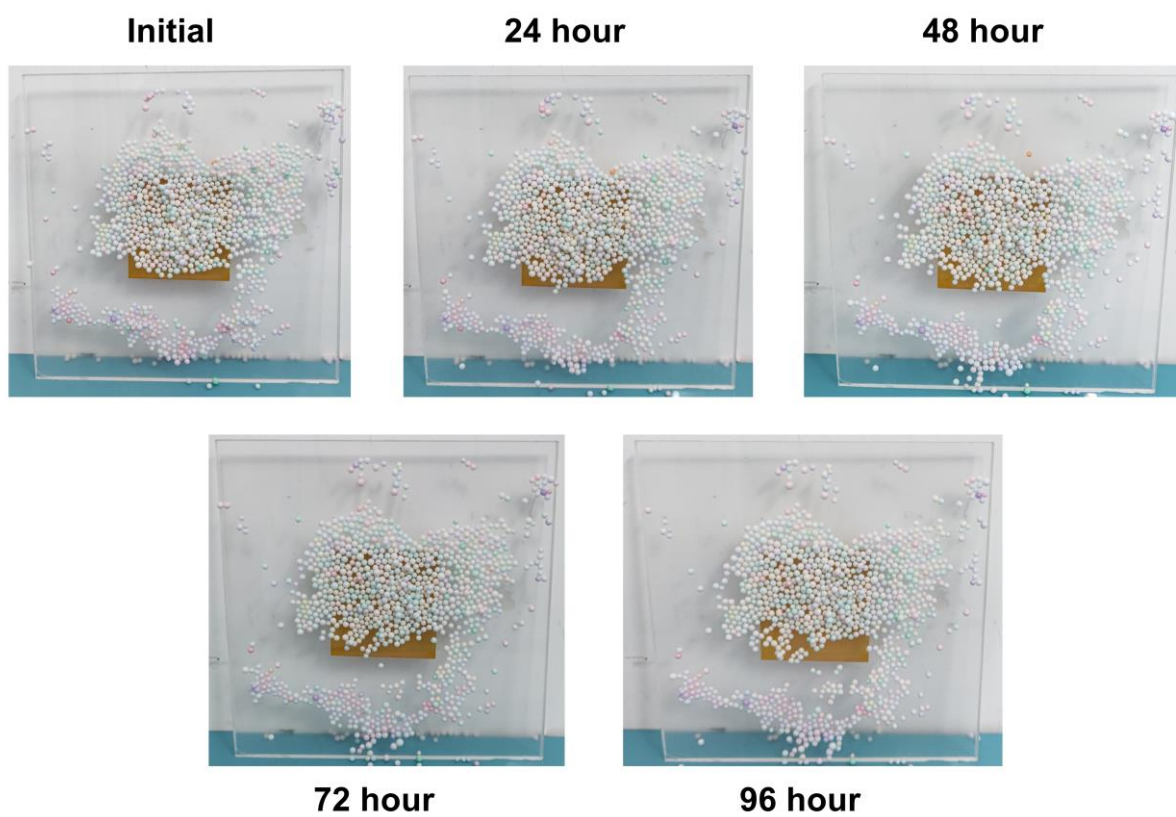
Figure S3. Optical photos of the PMMA with tiny balls adsorbed after 96 hours of statically vertical placement.
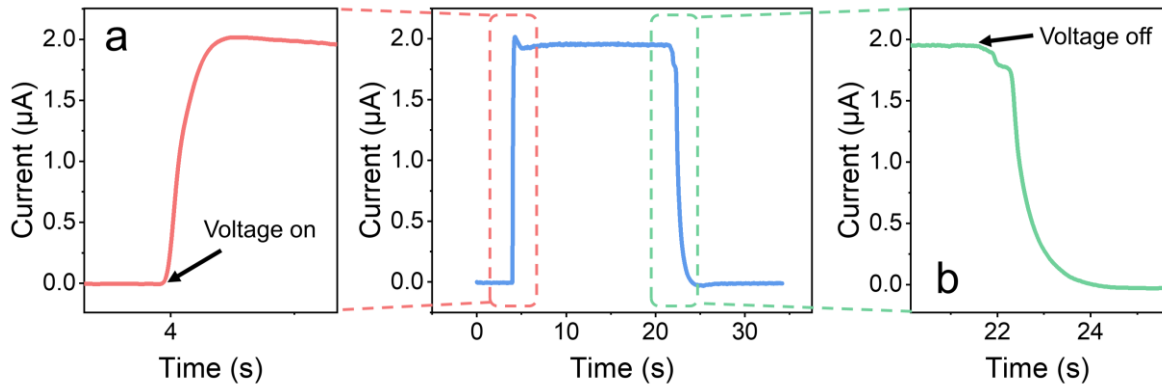
Figure S4. Complete leakage curve of PU material at a constant voltage of 3 kV. As shown in Fig. 2b, when the switch is closed, a constant voltage source set to 3 kV is immediately connected in series with the PU material. However, as shown in Fig. S4a, the current passing through PU slowly increases from 0 and takes some time to reach a stable state, indicating a time difference (phase difference) between the applied voltage and the generated current. Actually, PU is strictly an insulating material. Therefore, in the leakage test of Fig. 2b, the PU with electrodes attached on both sides has certain capacitive characteristics, which is the fundamental reason for the phase difference between the applied voltage and leakage current. Similarly, when the switch is disconnected (Fig. S4b), the current slowly drops to zero instead of immediately dropping to zero.
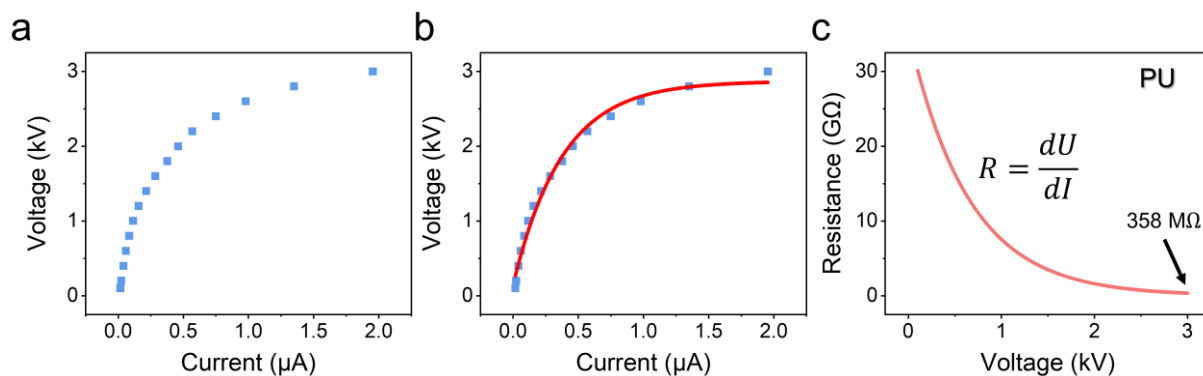
Figure S5. Variation curve of resistance with voltage. Firstly, we can obtain the leakage current of PU under different voltages (Fig. S5a). Then, fit Fig. S5a to obtain a continuous curve, as shown in Fig. S5b. Finally, the equation R=dU/dI is used to obtain the resistance at different voltages, as shown in Fig. S5c.
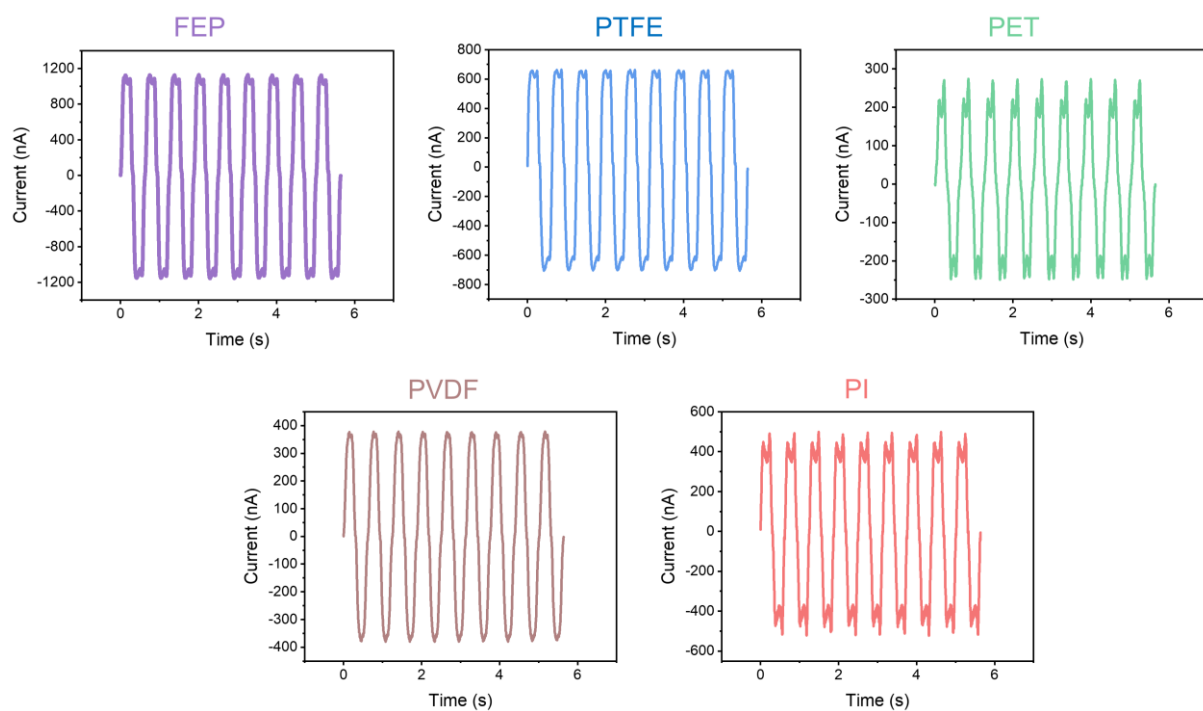
Figure S6. Specific output current waveforms of different slider materials.
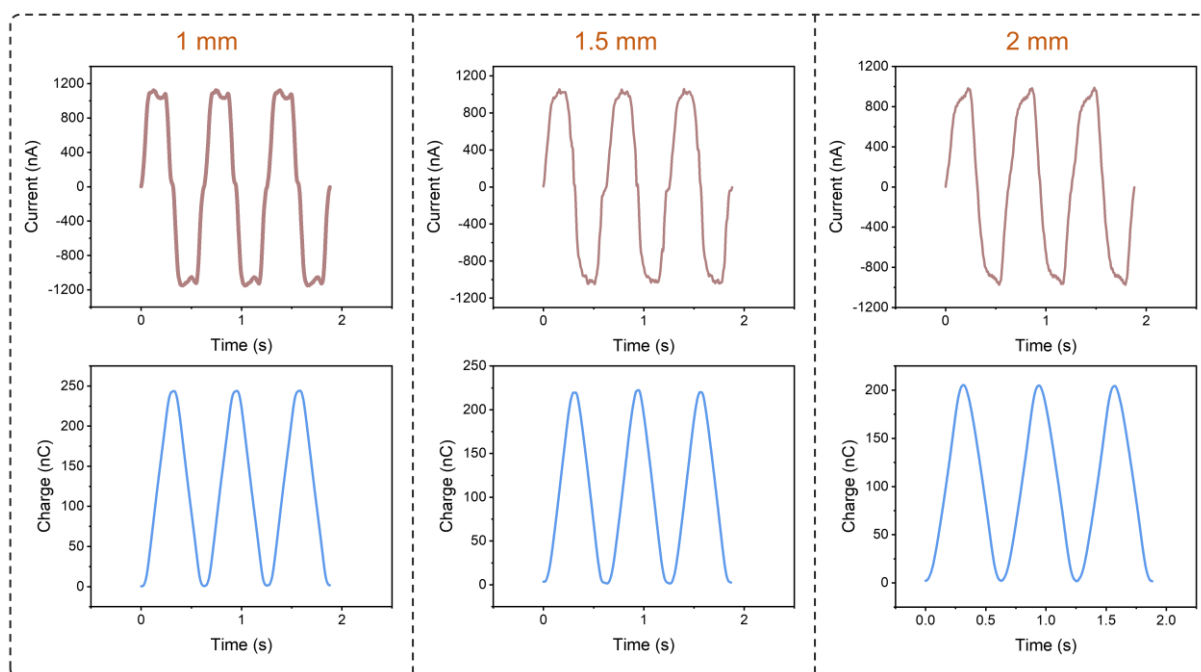
Figure S7. Dynamic output current and charge curves under different PU thicknesses.
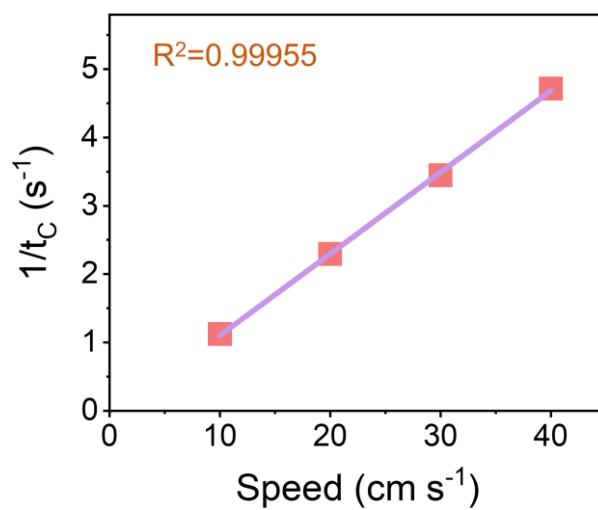
Figure S8. Inversely-proportional relationship between t_C and sliding speed.
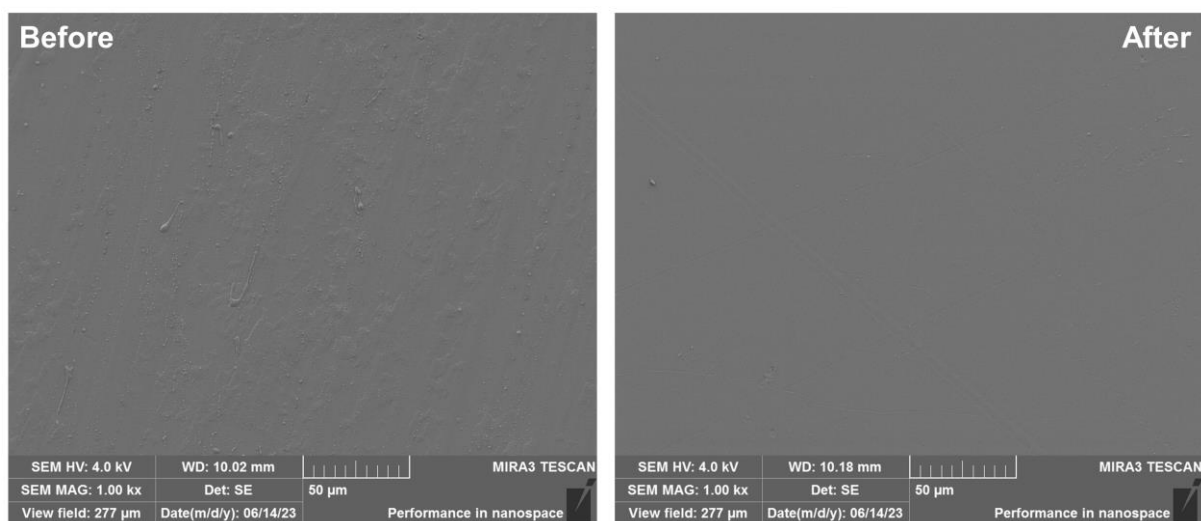
Figure S9. Comparison of surface morphology of FEP films before and after stability testing (SEM images).
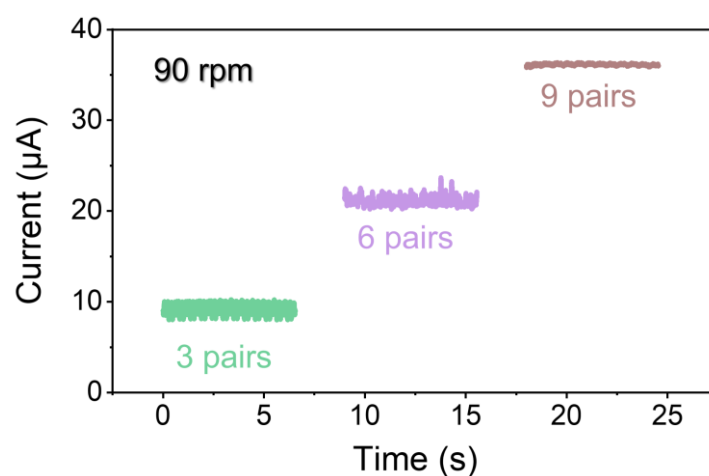
Figure S10. Output current of RHSC-TENG with different electrode pairs at a rotation speed of 90 rpm.
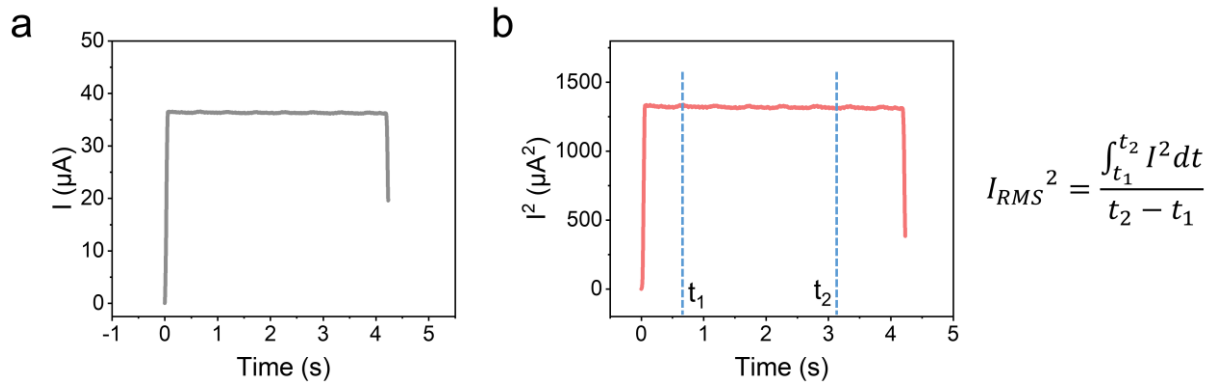
Figure S11. Specific calculation process for I_{RMS}. Fig. S11a shows the output current I(t) of RHSC-TENG after rectification under an external load of 2 MΩ. Based on this, we can further obtain I^2(t), as shown in Fig. S11b. Subsequently, the RMS current can be obtained by the following equation:

$$I_{RMS} = \sqrt{\frac{\int_{t_1}^{t_2} I^2 dt}{t_2 - t_1}}$$

The above I^2(t) and $\int_{t_1}^{t_2} I^2 dt$ are processed by ORIGIN software. Therefore, the RMS current of RHSC-TENG under an external load of 2 MΩ is calculated as 36.4 μA.
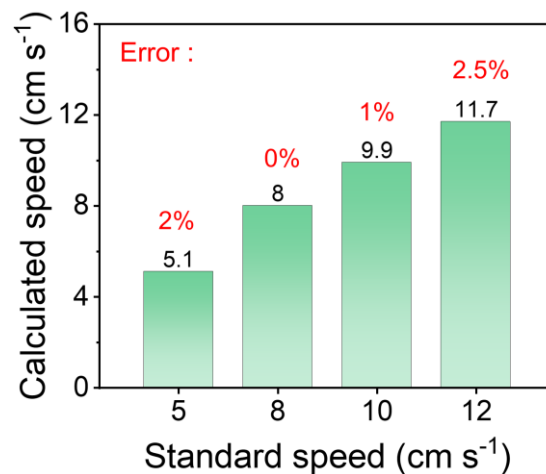
Figure S12. Calculated sliding speed.

Note S1. Detailed explanations and comparisons of different types of SC-TENGs.

Currently, there are four main strategies to obtain SC-TENGs:

First, the technology of collecting surface charge of tribo-layer by designing side electrode has been proposed for several years.[1-3] The strong electric field generated by the tribo-charge can induce the occurrence of electrostatic breakdown, thus forming a channel that can make the surface charge move directionally towards the side electrode. Therefore, the continuous local discharge can induce continuous charge transfer in external circuit and generate a constant DC output. This strategy achieves an ultra-high output charge density of 8.8 mC m^{-2}, efficiently achieving surface tribo-charge collection. However, SC-TENGs based on this strategy are very dependent on the surface states of dielectric materials, and their stability is seriously disturbed due to serious friction loss, which has not been solved yet.

Second, as we all know, the output of TENG based on triboelectrification and electrostatic induction coupling is a short pulse signal. Based on this, researchers obtained multiple pulse signals with phase differences through specific structural designs, and superimposed them into a stable DC output.[4-6] This strategy is very interesting. Nonetheless, processing multiple signals simultaneously poses many difficulties in connecting external leads.

Third, the researchers used three materials with different charge affinities as tribo-layers, achieving the effect of continuously transporting electrons from one material to another, thereby obtaining a constant potential difference in the external circuit.[7-9] This strategy selects electronic handling tools as a soft contact material, greatly improving the stability of the device. But, the stable implementation of this strategy relies on the system integration of multiple units, which undoubtedly has extremely high requirements for manufacturing processes. The two strategies mentioned above also face this difficulty and challenge.

Fourth, using semiconductor materials as tribo-layers is also a good solution to achieve stable DC output.[10-12] The built-in electric field generated by triboelectrification induces directional movement of electron-hole pairs, resulting in a unidirectional output signal in the external circuit. This strategy can generate sustained currents of up to milliamperes, but its low output voltage limits further improvement in output power. Besides, the low persistence of the output signal of SC-TENGs based on this principle is also a problem that needs to be addressed.

Above all, in the development history of SC-TENGs, how to obtain DC output effect through structural designs and further obtain constant current output form has always been a focus. **In this work**, more attention has been paid to the intrinsic output characteristics of materials, and the SC output effect has also been achieved in the form of AC output. This is a great attempt to break the limitations of traditional thinking and bring broader development

prospects for the progress of SC-TENGs. At the same time, the design of HSC-TENG using a common free-standing TENG structure is simple, which is beneficial for its widespread application. In addition, as shown in Fig. S2, the output waveform of the basic unit of HSC-TENG is also more stable.

Note S2. Design process of HSC-TENG as a speed sensor.

Step 1. The sliding of HCS-TENG is controlled by a linear motor (WEINERMOTOR WMU-090-D). The sliding speed can be accurately controlled at 5, 8, 10, and 12 cm s^{-1}.

Step 2. Use an electrometer (Keithley 6514) and a highly sensitive acquisition card (PCI-6259) to collect the current output signal of HCS-TENG, which is further transmitted to the computer.

Step 3. Use LabVIEW software to process the output signal of HCS-TENG and obtain a time (T) when the output current is greater than 100 nA.

Step 4. Divide the electrode width (4.25 cm) of HCS-TENG by the T obtained in step 3 to obtain the acquisition sliding speed. In attention, this step is also implemented by LabVIEW software.

Step 5. By comparing the accurate speed controlled in step 1 with the acquisition speed in step 4, the acquisition error of HCS-TENG as the speed sensor can be obtained.

Table S1. Output RMS power density comparison in the developmental stage of SC-TENGs.

Tribo-materials	Methods	RMS power density ($W\ m^{-2}$)	RMS power density ($W\ m^{-2}\ Hz^{-1}$)	References
PTFE/Nylon	Discharge	3	---	*Adv. Energy Mater.,* 2022, **12**, 2200963
PU/PTFE	Discharge	---	0.398	*Adv. Mater.,* 2023, **35**, 2208139
PVC/Cu	Discharge	0.2	---	*Nat. Commun.,* 2021, **12**, 4686
PU/PTFE	Discharge	---	3.29	*Energy Environ. Sci.,* 2023, **16**, 3486
Cu/PTFE	Multi-phase	1.11	0.271	*Energy Environ. Sci.,* 2021, **14**, 4523
PTFE/Nylon/fur	Ternary dielectric	8.77	3.508	*Adv. Energy Mater.,* 2023, **13**, 2202921
PET/PA/PTFE	Ternary dielectric	12.3	6.15	*Energy Environ. Sci.,* 2023, **16**, 3514
GaN/Bi$_2$Te$_3$	Tribovoltaic	11.85	9.23	*Adv. Mater.,* 2022, **34**, 2200146
Metal/Silicon	Tribovoltaic	0.15 mW m^{-2}	---	*Adv. Energy Mater.,* 2020, **10**, 1903713
GaN/Si	Tribovoltaic	1.5	---	*Energy Environ. Sci.,* 2022, **15**, 2366
FEP/PU	Charge migration	14.1	9.4	This work

Supplementary References

1   Z. Zhao, Y. Dai, D. Liu, L. Zhou, S. Li, Z. L. Wang and J. Wang, *Nat. Commun.*, 2020, **11**, 6186.

2   J. Zhang, Y. Gao, D. Liu, J.-S. Zhao and J. Wang, *Nat. Commun.*, 2023, **14**, 3218.

3   C. Shan, W. He, H. Wu, S. Fu, Q. Tang, Z. Wang, Y. Du, J. Wang, H. Guo and C. Hu, *Adv. Energy Mater.*, 2022, **12**, 2200963.

4   P. Chen, J. An, R. Cheng, S. Shu, A. Berbille, T. Jiang and Z. L. Wang, *Energy Environ. Sci.*, 2021, **14**, 4523.

5   X. Li, C. Zhang, Y. Gao, Z. Zhao, Y. Hu, O. Yang, L. Liu, L. Zhou, J. Wang and Z. L. Wang, *Energy Environ. Sci.*, 2022, **15**, 1334.

6   J. Wang, Y. Li, Z. Xie, Y. Xu, J. Zhou, T. Cheng, H. Zhao and Z. L. Wang, *Adv. Energy Mater.*, 2020, **10**, 1904227.

7   Q. Li, Y. Hu, Q. Yang, X. Li, X. Zhang, H. Yang, P. Ji, Y. Xi and Z. L. Wang, *Adv. Energy Mater.*, 2023, **13**, 2202921.

8   Q. Li, S. Fu, X. Li, H. Chen, W. He, Q. Yang, X. Zhang, H. Yang, D. Ren and Y. Xi, *Energy Environ. Sci.*, 2023, **16**, 3514-3525.

9   Q. Li, W. Liu, H. Yang, W. He, L. Long, M. Wu, X. Zhang, Y. Xi, C. Hu and Z. L. Wang, *Nano Energy*, 2021, **90**, 106585.

10   Z. Zhang, Z. Wang, Y. Chen, Y. Feng, S. Dong, H. Zhou, Z. L. Wang and C. Zhang, *Adv. Mater.*, 2022, **34**, 2200146.

11   Z. Zhang, D. Jiang, J. Zhao, G. Liu, T. Bu, C. Zhang and Z. L. Wang, *Adv. Energy Mater.*, 2020, **10**, 1903713.

12   Z. Wang, Z. Zhang, Y. Chen, L. Gong, S. Dong, H. Zhou, Y. Lin, Y. Lv, G. Liu and C. Zhang, *Energy Environ. Sci.*, 2022, **15**, 2366.